LANGMUIR

pubs.acs.org/Langmuir Article

Heterogeneous Dynamics of Sheared Particle-Laden Fluid Interfaces with Janus Particle Doping

Yiming Qiao, Zhengyang Liu, Xiaolei Ma, Nathan C. Keim,* and Xiang Cheng*



Cite This: Langmuir 2023, 39, 12032-12040



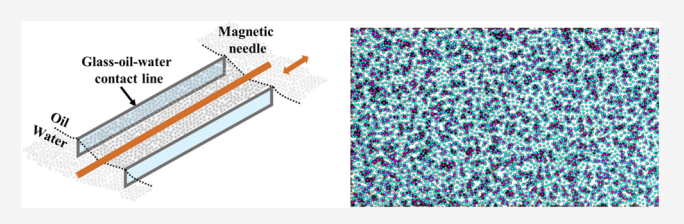
ACCESS I

III Metrics & More

Article Recommendations

Supporting Information

ABSTRACT: The formation of particle clusters can substantially modify the dynamics and mechanical properties of suspensions in both two and three dimensions. While it has been well established that large network-spanning clusters increase the rigidity of particle systems, it is still unclear how the presence of localized nonpercolating clusters affects the dynamics and mechanical properties of particle suspensions. Here, we introduce self-assembled localized particle clusters at a fluid—fluid interface by



mixing a fraction of Janus particles in a monolayer of homogeneous colloids. Each Janus particle binds to a few nearby homogeneous colloids, resulting in numerous small clusters uniformly distributed across the interface. Using a custom magnetic rod interfacial stress rheometer, we apply linear oscillatory shear to the particle-laden fluid interface. By analyzing the local affine deformation of particles from optical microscopy, we show that particles in localized clusters experience substantially lower shear-induced stretching than their neighbors outside clusters. We hypothesize that such heterogeneous dynamics induced by particle clusters increase the effective surface coverage of particles, which in turn enhances the shear moduli of the interface, as confirmed by direct interfacial rheological measurements. Our study illustrates the microscopic dynamics of small clusters in a shear flow and reveals their profound effects on the macroscopic rheology of particle-laden fluid interfaces. Our findings open an avenue for designing interfacial materials with improved mechanical properties via the control of formation of localized particle clusters.

■ INTRODUCTION

Clusters—small conglomerations of particles such as molecules, nanoparticles, or colloids—are ubiquitous in natural and engineering systems. Because of their intermediate sizes between microscopic and macroscopic scales, clusters frequently serve as a bridge linking the dynamics of isolated particles and the properties of bulk matter and have attracted immense research interest due to various intriguing properties they impart to bulk materials. ^{1–4} Particularly, the influence of clusters on the dynamics and mechanical properties of particle suspensions has been extensively studied for decades. ^{5–10} Recent studies have shown that the emergence of a network-spanning cluster can significantly increase the rigidity of a system, i.e., the ability of the system to resist imposed perturbations. ^{11–14} These percolating clusters are responsible for diverse phenomena ranging from the jamming transition of granular packings ^{15,16} to shear jamming and shear thickening of particle suspensions. ^{17–20}

While the structure—property relation of percolating clusters is much explored, few studies have investigated nonpercolating clusters of small sizes in particle suspensions. It remains elusive whether and how the dynamics and mechanical properties of a particle system are influenced by the presence of uniformly distributed localized clusters. The lack of experimental studies is partially due to the difficulty of controlling the size of particle clusters. Many factors can contribute to the formation of clusters in particle suspensions including hydrodynamic,²¹

electrostatic, ²² and capillary interactions, ²³ and applied shear. ¹⁴ The combined effect of these factors often results in a broad distribution of cluster sizes, making it hard to isolate the effect of small clusters on macroscopic system behaviors. In addition, probing the dynamics of localized clusters in bulk materials is challenging. Localized particle clusters are typically embedded inside opaque three-dimensional (3D) bulk suspensions. The temporal evolution of these clusters and their interactions with neighboring particles are typically fast on the time scale of single-particle dynamics. As a result, direct imaging of individual clusters in 3D suspensions requires special techniques with high-speed 3D imaging capabilities, ²⁴ which are not easily accessible.

Here, we overcome the above difficulties by studying the shear-induced dynamics of small particle clusters at the particle-laden fluid interfaces. Specifically, we control the assembly of localized clusters by adding a small amount of metallic-polymeric Janus particles in an otherwise uniform monolayer of homogeneous repulsive colloids at a fluid—fluid

Received: April 23, 2023 Revised: August 2, 2023 Published: August 17, 2023





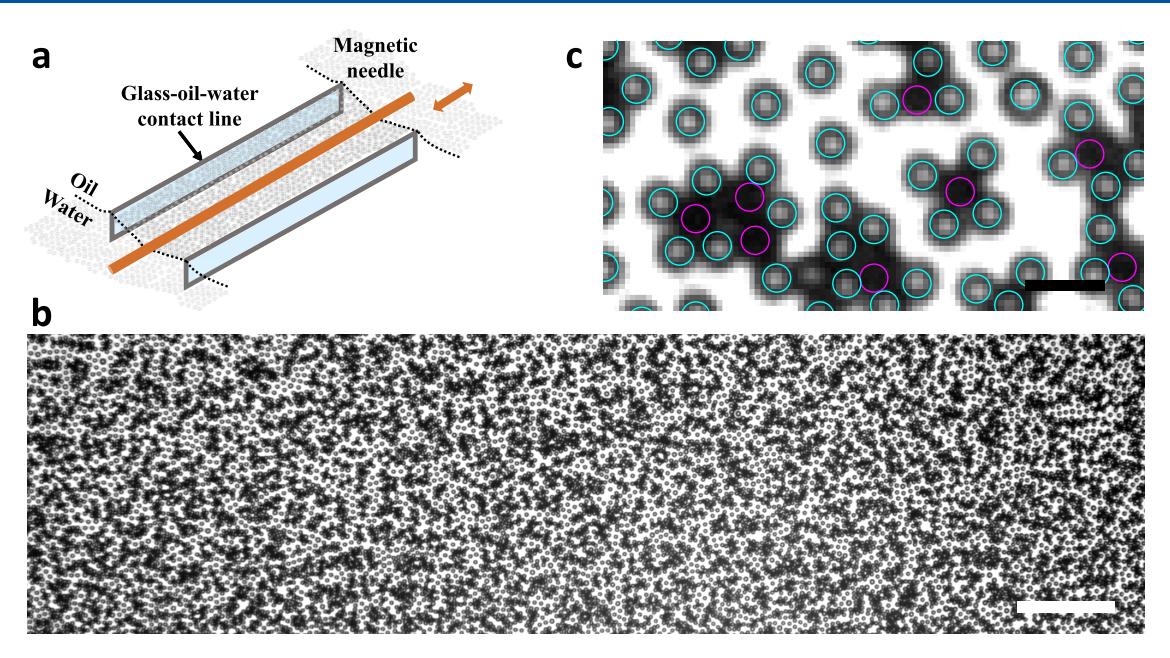


Figure 1. Apparatus and particle-laden fluid interface with Janus particle doping. (a) Schematic illustrating our custom magnetic rod interfacial stress rheometer (ISR). All of the relevant dimensions of the ISR are given in the text. (b) An optical microscopy image of a monolayer of PS spheres and PS-Pt Janus particles at the water-decane interface. The scale bar is 500 μ m. Black disks are Janus particles, and bright circles are PS spheres. (c) A zoomed-in image overlaid with the outcome of our particle finding. Magenta circles represent Janus particles from our particle finding, whereas cyan circles mark PS particles from our particle finding. The scale bar is 10 μ m.

interface. Thanks to their metallic hemisphere that reduces electric dipole repulsion, these Janus particles attract a single layer of homogeneous colloids via capillary forces, which give rise to small localized clusters distributed uniformly across the entire fluid interface.²⁵ We then apply linear oscillatory shear to such a specially prepared particle-laden fluid interface using a custom magnetic rod interfacial stress rheometer (ISR) and examine the shear-induced dynamics of particles at the interface. The two-dimensional (2D) nature of the fluid interface allows us to track the motions of all of the particles within and outside the clusters at high spatiotemporal resolutions. By analyzing the local affine deformation around individual particles, we find that the shear-induced particle dynamics at the fluid interface are heterogeneous: particles within clusters show stronger resistance to the imposed shear and experience less stretching, whereas those outside clusters endure more stretching beyond that imposed by external shear. Such heterogeneous dynamics are the direct consequence of the rigidity of clusters. We further hypothesize that rigid clusters protect a fraction of the interface in the interstitial space of clusters from stretching, which increases the effective surface coverage of particles and therefore enhances the shear moduli of the interface. We verify this hypothesis by correlating the microscopic configuration of particle clusters from direct imaging with the macroscopic rheology from interfacial rheometer measurements.

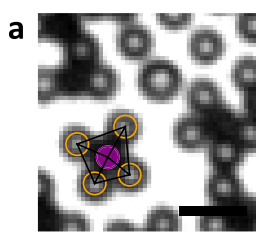
In addition to the generic effect of localized particle clusters on the mechanical properties of particle suspensions, our study also illustrates the unique dynamics of particle-laden fluid interfaces with Janus particle doping. As a special type of surface active agents, Janus particles have been widely used for modifying the physical and chemical properties of fluid interfaces (see refs 26-28 and references therein). In particular, the effect of Janus particles on the mechanical properties of fluid interfaces has been explored recently. $^{25,29-32}$ Our work complements these recent studies with direct

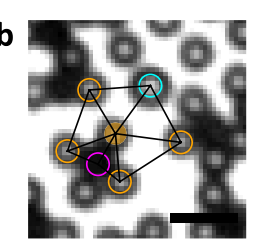
imaging of the microscopic dynamics of individual particles. The new approach and analysis adopted here reveal heterogeneous dynamics as the microscopic origin of the unusual mechanical strength of particle-laden fluid interfaces with Janus particle doping. As the density of particle clusters can be controlled via the doping concentration of Janus particles, our study demonstrates a convenient method for tuning the rheological properties of fluid interfaces, a feature desirable in a wide range of engineering applications. 33–36

■ EXPERIMENTAL SECTION

Interfacial Stress Rheometer (ISR). We use a custom-built magnetic rod interfacial stress rheometer (ISR) to impose linear shear on particle-laden fluid interfaces and measure their interfacial rheological response. ^{37–40} A trough $(10 \times 4 \times 5 \text{ cm}^3)$ is set on the stage of an inverted bright-field microscope (Nikon, Ti-E). A magnetic needle of radius 79.2 μm and length 2.45 cm is placed at the fluid interface between a pair of vertical glass walls (2 cm length, 6 mm width) in the center of the trough. Above the trough, we hang a pair of permanent magnets on a microscope slide whose field aligns the needle parallel to the glass walls. We use a single magnetic coil to generate a perturbative field, which drives the oscillatory motion of the needle at the fluid interface. Our observation window has a size of $1.330 \times 0.358 \text{ mm}^2$ and is located to one side of the needle, halfway along its length, as shown in Figure S1b of the Supporting Information (SI). By analyzing the oscillation of the needle in the window under the controlled perturbative field, we obtain the oscillation amplitude and phase shift of the needle in the controlled field, which allow us to calculate the storage and loss moduli of the fluid interface. Vibrations from external sources are weak at the particle-laden fluid interface and do not affect our ISR analysis (Figure S2). The schematic of the ISR setup is shown in Figure 1a with more details given in SI Section 1. The functionality, the calibration process, and the detailed calculation method can be further found in our previous publication on the design of the ISR.⁴⁰

Particle-Laden Fluid Interface with Janus Particle Doping. Two types of colloidal particles are used in our study. Monodisperse surfactant-free sulfate-modified polystyrene (PS) spheres with a





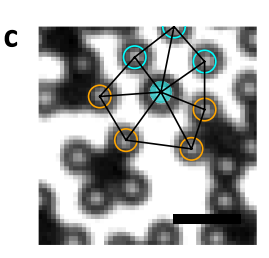


Figure 2. Three classes of particles at the interface. (a) Class (1): a Janus particle at the core of a cluster. (b) Class (2): a PS sphere at the edge of a cluster, which is surrounded by a Janus particle as well as PS spheres within and outside clusters. (c) Class (3): an isolated PS sphere, which is surrounded by PS spheres within and outside clusters. The black lines are the Delaunay triangulation of the particles of interest (highlighted by solid disks). The open circles represent the neighboring particles based on the Delaunay triangulation (magenta for Janus particles, brown for PS spheres in clusters, and cyan for isolated PS spheres outside clusters). The scale bars are $10 \mu m$.

diameter of 4.1 μ m were purchased from Thermo Fisher Scientific. The spheres are used as homogeneous colloids at fluid interfaces and also as the basis for synthesizing Janus particles. Following the published protocol, ^{25,41,42} PS—platinum (PS—Pt) Janus particles are fabricated by drop-casting of the PS spheres on a glass substrate into a monolayer and sputtering deposition of a thin film of Pt on the upper surface of the PS spheres. The scheme of the process and the scanning electron microscopy images of the PS—Pt Janus particles are shown in Figure S3 in the SI. The thickness of the Pt coating is ~20 nm, which is controlled through the coating time based on a calibration curve at the given deposition rate. The coating thickness within the range of 10-240 nm shows no effect on the interparticle interactions and the microstructure of the interface. ²⁵

To assemble a particle-laden fluid interface with Janus particle doping, we first prepare a suspension of homogeneous PS spheres and Pt–PS Janus particles in a mixture of reagent grade alcohol (50% w/v, VWR International) and distilled deionized water (Millipore Direct-Q3, 18.2 M Ω ·cm at 25 °C). The ratio between PS and Janus particles is fixed at 4:1 unless stated otherwise. The volume fraction of the suspension is ~5%. A clean water—decane interface is next prepared by adding 10 mL of water as the subphase and 10 mL of decane (Sigma-Aldrich) as the superphase. We then gently place the magnetic needle at the clean water—decane interface with tweezers. Afterward, we slowly deposit the well-sonicated particle suspension at the interface. Particles quickly spread out along the interface and form a stable interfacial particle monolayer thanks to their high detachment energy. $^{33,43-45}$

Without Janus particles, PS spheres alone form hexagonal crystals at the fluid interface due to the interparticle repulsion induced by the electric dipoles of particles at the interface ^{25,46–50} (Figure S4). The metallic surface of Janus particles modifies the charge distribution on the particles and lowers the strength of electric dipoles (Figure S4b), which therefore reduces the repulsion between Janus particles and PS spheres. As a result, capillary attraction dominates the interaction between Janus particles and PS spheres, giving rise to localized particle clusters. A detailed discussion of the interparticle interactions can be found in SI Section 3. A quantitative analysis of the competition between different interparticle interactions at fluid interfaces can be further found in refs 25,46. Because of the nature of the interparticle interactions discussed above, a typical particle cluster has a Janus particle at the core surrounded by a single layer of 2-5 PS spheres. These small clusters are uniformly dispersed throughout the fluid interface (Figure 1b). Thus, at a macroscopic scale beyond the characteristic length of clusters, the interface remains uniform and isotropic. We fix the area fraction of the particle monolayer at $\phi = 31.8\%$. Such an intermediate ϕ is chosen so that the rheological signature of the layer is above the resolution of our ISR, and particles are not too crowded at the interface for more accurate particle finding and tracking. Interfaces at different ϕ are also tested, which yield qualitatively similar results with stronger noise (see the Results and Discussion Section).

Before each experiment, we apply a large amplitude oscillatory shear of strain $\sim\!20\%$ and frequency 1 Hz for 10 min to eliminate any potential nonuniform structures and reset the initial condition of the

interface. After stopping the shear, we wait for another 10 min until no further particle motions are observed before starting the experiment at a controlled frequency and stress. Unless stated otherwise, we fix the shear frequency at f=1 Hz and vary the shear stress amplitude by controlling the strength of the perturbative magnetic field.

Image Processing. The interface is imaged through a 10× objective (Nikon, NA 0.30, WD 17.0 mm) on the inverted microscope with a synchronized high-resolution CMOS camera (Basler acA2040–90 um USB 3.0). A typical image is shown in Figure 1b, where the brighter particles are PS spheres and the darker particles are PS–Pt Janus particles. We write a custom Python code to distinguish and find the centers of PS spheres and Janus particles. Figure 1c shows a representative particle finding result, with two different types of particles marked separately. The details of the particle finding algorithm can be found in SI Section 4 and in ref 51. After the centers of all of the particles are identified at different frames, we use the open-source software "trackpy" to track the trajectories of the particles. To reduce tracking errors, we discard any particle trajectories that are not tracked continuously over the entire readout process.

■ RESULTS AND DISCUSSION

The particle-laden fluid interface is sheared using our custom ISR. Specifically, sinusoidal stress is applied to the needle through the perturbative field of the magnetic coil, which induces an oscillatory shear strain (with a phase lag) on the particle monolayer between the two glass walls (Figure 1a). We vary the applied stress via the amplitude of the perturbation current, which yields strain amplitudes ranging from 0.006 to 0.104. The detailed calculation of the stress (via the current in the coil) and the strain (via the motion of particles) is discussed in SI Section 5. While the macroscopic interfacial rheology can be derived from the stress—strain relation, the microscopic dynamics of particles are obtained through the simultaneous imaging of ~10,000 particles at the sheared interface.

To quantify the microscopic dynamics of particles, we compare the relative positions of the nearest neighbors of a particle at the two instants t_0 and t. Here, the nearest neighbors are determined through Delaunay triangulation (Figure 2). We distinguish three different classes of particles within the monolayer based on the particle type (PS vs Janus) and whether they are in clusters: (1) Janus particles in clusters (Figure 2a); (2) PS spheres in clusters (Figure 2b); and (3) isolated PS spheres outside clusters (Figure 2c). Note that as Janus particles attract PS spheres nearby, they are always in clusters. Accordingly, an independent class of Janus particles outside clusters does not exist. We detect particle clusters by binarizing raw images, choosing a proper threshold that includes the pixels between connected particles. The details of

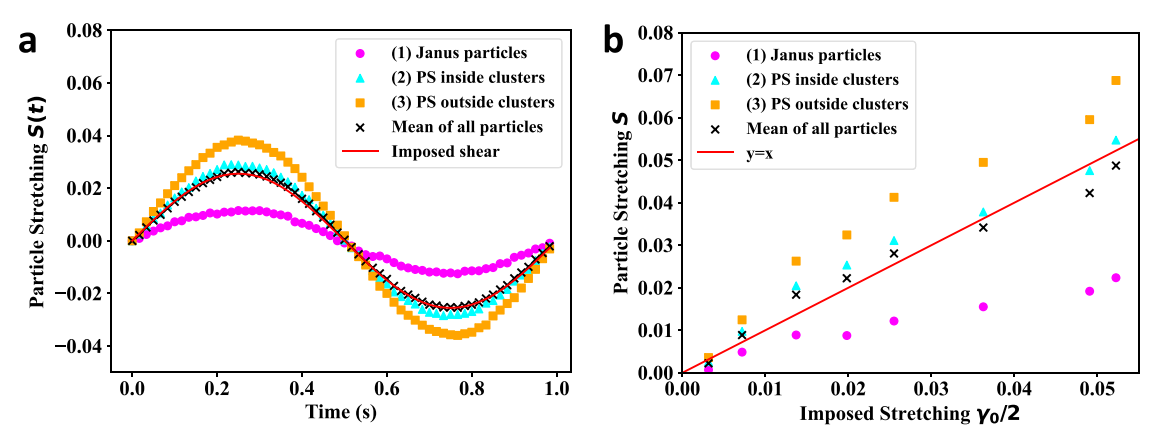


Figure 3. Local stretching of particles. (a) Average stretching experienced by the three classes of particles as a function of time over one shear cycle. The average local stretching of all particles and the stretching that corresponds to the imposed linear shear $(\gamma/2)$ are also plotted. (b) The amplitudes of the oscillatory local stretching of different classes of particles as a function of the imposed stretching amplitude $\gamma_0/2$. The red line represents y = x.

the detecting procedure are illustrated in Figure S5 and discussed in SI Section 4.

For a particle of a given class, we calculate the local deformation gradient tensor of the particle ε_{ij} by minimizing the mean-square difference between the relative displacements of the nearest neighbors of the particle and the relative displacements that the neighbors would have under a pure affine deformation ε_{ij}^{54}

$$D^{2}(t_{0}, t) = \sum_{n=1}^{N_{NN}} \sum_{i=1}^{2} \left(r_{n}^{i}(t_{0}) - r_{0}^{i}(t_{0}) - \sum_{j} (\delta_{ij} + \varepsilon_{ij}) [r_{n}^{j}(t) - r_{0}^{j}(t)] \right)^{2}$$
(1)

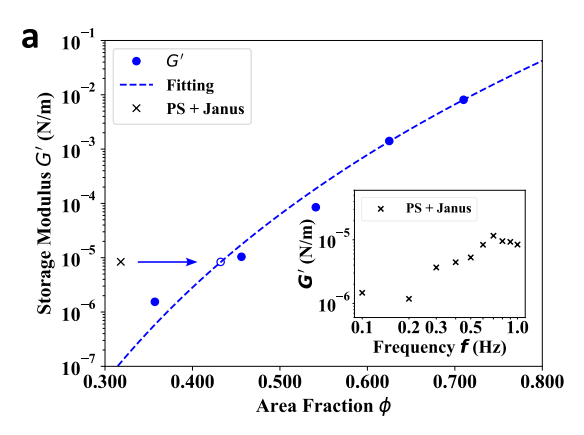
where indices i and j refer to the two spatial Cartesian coordinates at the interface and the index n runs over all of the nearest $N_{\rm NN}$ neighbors of the particle in question (n=0 at $\vec{r}_0)$. Here, the x axis is along the motion of the needle, and the y axis is along the shear gradient direction. The local stretching experienced by the particle between the reference frame t_0 and time t is given by $S=(\varepsilon_{12}+\varepsilon_{21})/2$, whereas the local rotation of the particle is $\Omega=(\varepsilon_{12}-\varepsilon_{21})/2$. The minimum of D^2 , $D^2_{\rm min}$, characterizes the local deviation of the particle dynamics from affine deformation. The analysis of nonaffine motion via $D^2_{\rm min}$ was originally invented by Falk and Langer for quantifying the viscoplastic deformation of amorphous solids and has been employed previously in analyzing the dynamics of homogeneous particle monolayers. 50,55,56

Local Stretching. We first focus on the local stretching S(t) experienced by individual particles, a key quantity characterizing particle dynamics under shear and determining the shear moduli of the interface. We choose the reference state at t_0 when the imposed shear stress on the needle is zero. Selecting a different reference state results in a phase shift of S(t) but does not change its amplitude and oscillation frequency (Figure S7). Figure 3a shows the temporal variation of S(t) averaged over each of the three classes of particles, $\langle S(t) \rangle_{k}$ within one shear cycle at an imposed strain amplitude $\gamma_0 = 0.05$, where the subscript k = 1, 2, 3 indicates the three classes of particles defined above. As expected, $\langle S(t) \rangle_k$ varies sinusoidally at the frequency f of the imposed shear. The average stretching of all of the particles, $\langle S(t) \rangle$, is determined by the imposed shear, following $\langle S(t) \rangle = (\gamma_0/2) \sin(2\pi f t)$. Note that the linear shear of the needle can be decomposed into a stretching component and a rotation component of equal strengths, which accounts for the one-half factor in the amplitude. More interestingly, particles within clusters show substantially weaker stretching (Figure 3a). In particular, as Janus particles are located at the core of clusters, they endure the lowest stretching among all three classes of particles.

Such heterogeneous dynamics are independent of the amplitude of the imposed shear strain. At each applied strain amplitude γ_0 , we measure the amplitudes of the oscillatory local stretching experienced by different classes of particles, $\langle S \rangle_k$ (Figure 3b). $\langle S \rangle_k$ for all three classes increases linearly with the imposed stretching of applied shear $\gamma_0/2$ but with noticeably different slopes α_k . For isolated PS spheres, $\langle S \rangle_3$ = α_3 ($\gamma_0/2$) with $\alpha_3 = 1.35 \pm 0.14 > 1$ at a confidence level of 95%. These particles experience stretching 35% higher than that imposed by linear shear. In comparison, PS spheres in clusters have $\alpha_2 = 1.06 \pm 0.10$, close to the imposed stretching. For Janus particles, the slope is smallest at $\alpha_1 = 0.43 \pm 0.04 <$ 1. The results show that nonpercolating particle clusters resist the stretching imposed by the shear. Near the center of the clusters, particles experience the weakest stretching. Finally, when averaging over all of the particles at the interface, we have $\langle S \rangle = \alpha(\gamma_0/2)$ with $\alpha = 0.95 \pm 0.09$. Thus, the average behavior of all of the particles is determined by the imposed linear shear.

The presence of heterogeneous dynamics is also independent of particle concentrations and PS/Janus particle ratios. Results of $\langle S \rangle_k$ for two additional particle-laden fluid interfaces with different ϕ and PS/Janus ratios are shown in Figure S8. In both cases, the stretching of the particles in clusters is weaker than that of the imposed shear. Janus particles, being at the core of the clusters, experience the lowest stretching. The slopes of $\langle S \rangle_k$ versus the stretching of the imposed shear $\gamma_0/2$ of the three classes of particles also follows qualitatively similar trends. Note that the data at both low ϕ and high ϕ show stronger fluctuations compared with the data at the intermediate ϕ (Figure S8). While the noise of the low- ϕ result originates from the statistical fluctuation due to the small number of particles tracked at the interface, the noise of the high- ϕ result arises from the errors in particle finding and tracking at high concentrations.

Interfacial Rheology. The heterogeneous dynamics suggest that particle clusters formed by the capillary attraction between Janus particles and PS spheres are semirigid against the interfacial shear flow. The rigidity of clusters under shear



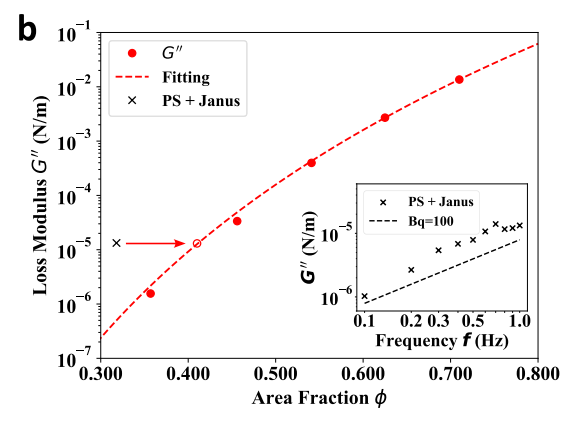


Figure 4. Interfacial storage modulus G' (a) and loss modulus G'' (b) of monolayers of homogeneous PS spheres of different area fractions ϕ at a fixed shear frequency of 1.0 Hz. Shear strains are less than 0.1% in the linear viscoelastic regime. The data (solid disks) are from ref 40. The dashed lines are power-law fits to guide the eye. The crosses at $\phi = 31.8\%$ indicate the moduli of the Janus-doped interface in this study, which are equal to the moduli of the monolayers of homogeneous PS spheres at higher effective area fractions, as indicated by the open circles. Insets: a frequency sweep of G' and G'' of the Janus-doped interface. The black dashed line indicates a constant Boussinesq number Bq = 100.

has important implications for interfacial rheology. To understand the relation between the dynamics of particle clusters and the rheology of the particle-laden fluid interface, we measure the storage and loss moduli of the interfaces, G'and G'', at different shear frequencies f in the linear viscoelastic regime (Figure 4, insets). Specifically, the complex shear modulus of interface G is first calculated as the ratio of oscillating stress and strain. The real and imaginary parts of G then give G' and G'', respectively. The detailed calculation method is presented in SI Section 5. The moduli increase with f, a trend agreeing well with previous studies at higher particle area fractions.²⁵ At shear frequency f = 1 Hz, the storage modulus of the Janus-doped interface G' is about 2 orders of magnitude higher than that of the homogeneous PS interface of the same area fraction (Figure 4a). Thus, the interface decorated with small clusters is, on a macroscopic scale, more rigid than the interface without clusters. For accurate interfacial rheology measurements, the force on the probe (the needle in our case) should be dominated by the force from the interface, rather than from the bulk fluids.³⁹ To quantify the ratio of the shear force from the interface to the viscous drag from the bulk fluids, a dimensionless Boussinesq number, $Bq \equiv G''/(f\eta_b r)$, is often evaluated, where η_b is the viscosity of bulk fluids and r is the size of the probe. In our system, $r = 79.2 \mu m$ is set by the radius of the needle, and $\eta_{\rm b}=0.001~{\rm Pa\cdot s}$ is the viscosity of water. With the measured G'', we have Bq>100 for the Janusdoped particle interface (Figure 4b, inset), ensuring the validity of our results.39

How do localized rigid particle clusters modify the interfacial rheology of the interface? As the motion of the portion of the interface in the interstitial space between particles in clusters or at the close proximity of clusters is entrained to the motion of the clusters, this portion of the interface is not stretched strongly by shear either (Figure 5a). Thus, the presence of nonpercolating clusters effectively increases the surface coverage of particles at the interface. By definition, the area fraction of particles at the interface is $\phi = N\pi d^2/(4A)$, where N is the total number of particles, πd is the length of the contact line of a single particle at the interface, and A is the total surface area of the interface. If the contact angle of particles is close to 90°, d can be approximated as the diameter of particles. The effective area fraction due to the presence of particle clusters can be written as

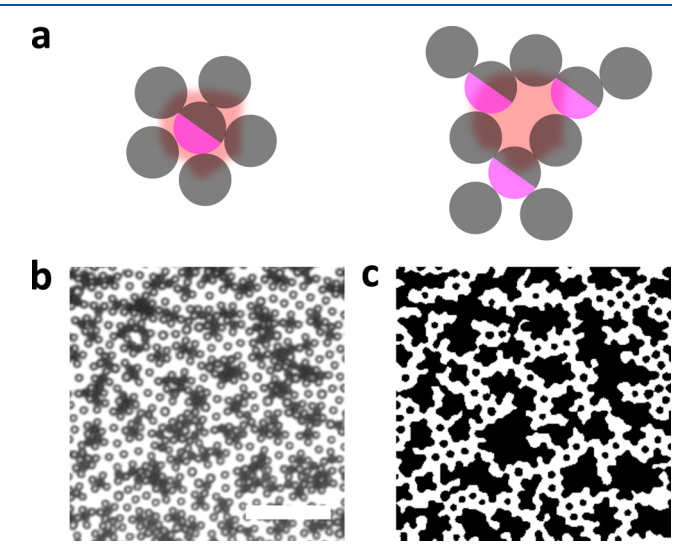
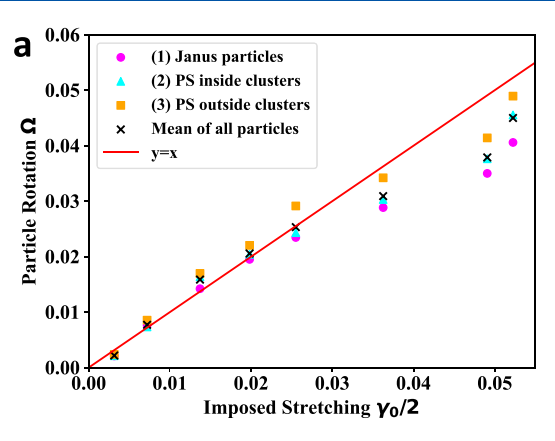


Figure 5. Configurations of particle clusters. (a) Schematics of possible configurations of particle clusters. The gray disks represent PS spheres, and the purple half-disks represent Pt-coated areas of the Janus particles. The shaded red areas illustrate the part of the fluid interface that is protected by the clusters and therefore not subject to strong stretching by shear. Hence, the red regions should be considered as a part of the clusters and remain rigid under shear, which increases the effective particle area fraction. The typical length scale of the empty space enclosed inside clusters in the right configuration is on the order of the size of a particle. (b) Raw image of a particle-laden interface. Scale bar: 50 μ m. (c) The processed image after applying a binary threshold and incorporating the entrained interface within clusters. The image is used to calculate the effective area fraction of the interface $\phi_{\rm eff}$.

$$\phi_{\text{eff}} = \frac{N\pi d_{\text{e}}^2}{4A} = \frac{N\pi (d + \delta d)^2}{4A}$$
(2)

where $d_{\rm e}$ is the effective diameter of particles due to the extra entrained interface and $\delta d \equiv (d_{\rm e}-d)$ gives the effective increase of the diameter of particles at the interface with localized clusters. It is easy to see that

$$\frac{\delta d}{d} = \left[\left(\frac{\phi_{\text{eff}}}{\phi} \right)^{1/2} - 1 \right] \tag{3}$$



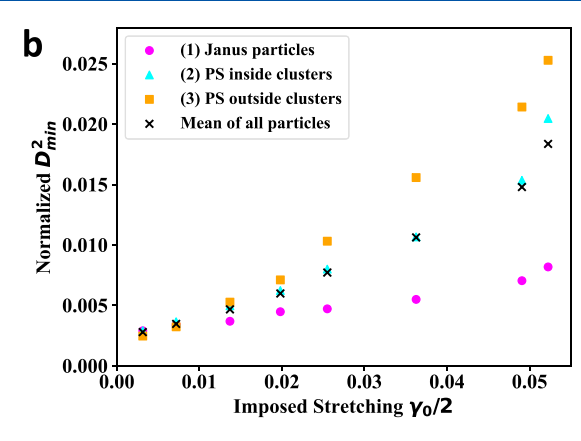


Figure 6. Local rotation and nonaffine deformation of particles. (a) The amplitudes of the local rotation of different classes of particles as a function of the rotation imposed by the linear shear $\gamma_0/2$. The red line indicates that y = x. (b) The amplitudes of the normalized D_{\min}^2 of different classes of particles as a function of the imposed shear. The crosses show the average over all particles.

We estimate δd using two different methods. Macroscopically, we compare the moduli of the Janus-doped interface to the interface of homogeneous PS spheres. The elastic modulus of the Janus-doped interface of $\phi = 31.8\%$ is equivalent to that of the homogeneous interface at an elevated area fraction of ϕ = 43.2% (Figure 4a) with an increase of $\sim 30\%$, which gives $\delta d/d = 0.17$ based on eq 3. Note that the effective area fraction would be $\phi_{\rm eff}$ = 41.2% if we compare the G'' of the Janusdoped interface and G'' of the homogeneous interface (Figure 4b), which gives a slightly smaller $\delta d/d = 0.14$. Microscopically, we identify particle clusters from microscope images and obtain the effective area occupied by clusters, including the interstitial space of the clusters (Figure 5b,c). The effective area fraction calculated from the image analysis is 55.2%, which yields $\delta d/d = 0.32$. Thus, both methods indicate an increase of the effective area fraction and show a qualitatively similar trend in the increase of the effective size of particles due to the formation of clusters. The discrepancy in $\delta d/d$ may be due to each method's systematic errors: the image analysis likely overestimates the effective area fraction due to the finite resolution and aberration of optical microscopy close to particles, which introduce a large uncertainty in selecting the threshold for cluster analysis (Figure S5). More importantly, as the entrained interface is not completely rigid due to the finite deformation of clusters under shear (Figure 3), the image analysis assuming rigid entrained interfaces also overpredicts the effective size of particles compared with that from the rheological tests.

Our analysis provides a qualitative explanation of the increase of the interfacial loss modulus G'' of the Janusdoped interface. With $\phi_{\rm eff} > \phi$, a larger portion of the interface resists the shear flow. The stronger distortion of the shear flow increases the dissipation of the system and therefore the interfacial viscosity and G'' of the interface. It is worth noting that the presence of nonpercolating clusters also increases the effective volume fraction of 3D suspensions at low to intermediate volume fractions, which leads to a gradual increase of suspension viscosity with shear—an effect known as continuous shear thickening—due to the formation of hydroclusters at high shear rates. 24,57

Two possible mechanisms, which are not mutually exclusive, could explain the increase in the storage modulus G' and thus interfacial elasticity:

(1) The elasticity of a homogeneous PS particle monolayer arises from the electrostatic repulsion between particles.

Imposed shear reduces the distances between particles along the major compressive axis of the shear against the interparticle electrostatic repulsion, which converts the mechanical energy of the imposed shear into the electrostatic potential energy and gives rise to the elasticity of the interface. The formation of Janus-PS clusters does not eliminate the electrostatic repulsion between isolated particles and between clusters. In fact, the strength of the electrostatic repulsion between clusters even increases due to the aggregation of PS spheres. Through experiments and theory, Petkov and co-workers have demonstrated the enhanced electrostatic repulsion due to the formation of compact clusters of charged particles at fluid interfaces, which outweighs the increased distance between particles and increases the surface pressure of particle-laden fluid interfaces.⁵⁸ We note that in ref 58, surface pressure is found to scale as the square root of the number of particles in each aggregate, weaker than the enhancement of shear moduli here. In our system, as the stretching around particles inside clusters is reduced owing to the rigidity of the clusters, the stretching of material between clusters must increase above the average to match the imposed shear (Figure 3). Such an increased stretching, in combination with the enhanced electrostatic repulsion between clusters, promotes a drastic increase in the elastic response of the interface.

(2) Particle clusters often have noncircular shapes with corners and edges (Figures 1b and 5b). Under imposed shear, the rotations of nearby clusters are coupled, which facilitates the formation of percolating force chains along the compressive axis of the shear. The formation of these shear-induced structures enhances the elasticity of the interface.¹⁷ Note that these shear-induced force chains are different from static percolating particle clusters, which are independent of shear compression and do not exist in our system.

Local Rotation and Nonaffine Deformation. Lastly, we also investigate local rotation and local nonaffine deformation at the interface. Figure 6a shows the amplitudes of the oscillatory local rotation of particles averaged within each of the three classes of particles, $\langle \Omega \rangle_k$, at different imposed shear strains. Interestingly, although the local stretching experienced by different classes of particles is different, the local rotations of particles' neighborhoods are similar independent of particle classes. The rotation of particles is dictated by the rotation component of the linear shear, following $\langle \Omega(t) \rangle_k = (\gamma_0/2) \sin(2\pi f t)$. Hence, while the stretching of particles is

heterogeneous due to the presence of localized clusters, the rotation of particles remains uniform.

Figure 6b shows D_{\min}^2 as a function of $\gamma_0/2$, which quantifies the degree of local nonaffine deformation at different imposed shear strains. To compare the degree of nonaffine deformation of different particles as well as particles in different systems, D_{\min}^2 needs to be normalized properly. Thus, we first calculate the average distance between a particle and its closest neighbors L and compute the average for each class of particles $\langle L \rangle_k$. We then normalize D_{\min}^2 by the number of nearest neighbors N_{NN} and the square of the average distance over different classes of particles, $\langle D_{\min}^2/N_{\text{NN}}\rangle_k/\langle L\rangle_k^2$. Independent of the class of particles, the degree of nonaffine deformation shows a nonlinear increase with increasing γ_0 . Larger strains generally result in stronger nonaffine deformation. 49,50,55,56 Similar to the local stretching, the nonaffine deformation is also heterogeneous. PS spheres outside clusters show the largest nonaffine deformation, whereas Janus particles within clusters have the smallest nonaffine deformation. This difference is also apparent when comparing to previously studied undoped interfaces with bidisperse and monodisperse particles, 50,59 where the mean D_{\min}^2 at imposed stretching $\gamma_0/2$ = 0.05 would be \sim 0.01—roughly half of the corresponding measurement outside clusters in the present study.

CONCLUSIONS

In this study, we imaged the shear-induced dynamics of particles at a particle-laden fluid interface composed of a mixture of homogeneous PS spheres and PS-Pt Janus particles. Due to the reduced electrostatic repulsion between the PS spheres and the Janus particles, a large number of localized nonpercolating particle clusters form at the interface, which have a typical configuration with a Janus particle at the core and PS spheres at the rim of the clusters. By analyzing the local affine deformation of individual particles under imposed oscillatory linear shear, we showed that the dynamics of the interface are heterogeneous. In particular, we found that PS spheres outside clusters endure the largest shear stretching among all of the particles at the interface and show the strongest nonaffine deformation, whereas Janus particles inside clusters experience the least stretching and have the smallest nonaffine deformation. The stretching and nonaffine deformation of PS spheres inside clusters are intermediate between these two limits. In comparison, the rotational dynamics of the interface is homogeneous and dictated by the imposed linear shear, independent of the type of particles.

We also explored the effect of localized particle clusters on the mechanical strength of the interface. Using a custom interfacial rheometer, we showed that the heterogeneous dynamics induced by particle clusters increase the macroscopic rigidity of the interface and substantially enhance its interfacial shear moduli. We propose that such an increase in interfacial shear moduli can be understood from the elevated effective area fraction associated with the formation of rigid particle clusters. It has been well established that network-spanning clusters can increase the rigidity of particle systems. S,112-14 Our study showed that small localized rigid particle clusters can also increase the rigidity of particle systems by increasing effective particle concentrations. The finding is potentially useful to improve the stability of interface-rich materials such as Pickering emulsions.

An interesting open question is how the degree of cluster rigidity affects macroscopic rheology. Although it is relatively

easy to change the number density of particle clusters by controlling the number ratio of PS to Janus particles, it is more difficult to vary the size and rigidity of particle clusters. Adding surfactants and varying the pH and salt concentration of the aqueous phase have been shown to be effective in altering interparticle interactions at fluid interfaces, 46-48 which may be combined with Janus particles to achieve a more comprehensive control of the structure and the mechanical properties of particle clusters at particle-laden fluid interfaces. Semirigid particle clusters with weak bonding between particles may modify the moduli of an interface in a nonlinear fashion and give rise to a time-dependent rheological response due to the dynamic breaking and reformation of particle bonding under shear. 63 Lastly, Pt-PS Janus particles become active and selfpropel when submerged in hydrogen peroxide solutions, providing a model system to study the rheology of active fluids. 64,65 Recent studies have shown that active Janus particles can decrease the shear moduli and yield stresses of 3D colloidal gels. 66,67 How the activity of Janus particles modifies the shear moduli and the viscoelasticity of fluid interfaces remains unexplored.

ASSOCIATED CONTENT

Solution Supporting Information

The Supporting Information is available free of charge at https://pubs.acs.org/doi/10.1021/acs.langmuir.3c01085.

Further information on experimental details; materials and methods; and the effect of particle concentrations (PDF)

AUTHOR INFORMATION

Corresponding Authors

Nathan C. Keim — Department of Physics, Pennsylvania State University, University Park, Pennsylvania 16802, United States; Email: keim@psu.edu

Xiang Cheng — Department of Chemical Engineering and Materials Science, University of Minnesota, Minneapolis, Minnesota 55455, United States; oorcid.org/0000-0002-2759-764X; Email: xcheng@umn.edu

Authors

Yiming Qiao — Department of Chemical Engineering and Materials Science, University of Minnesota, Minneapolis, Minnesota 55455, United States; orcid.org/0000-0002-1917-2588

Zhengyang Liu – Department of Chemical Engineering and Materials Science, University of Minnesota, Minneapolis, Minnesota 55455, United States

Xiaolei Ma — Department of Chemical Engineering and Materials Science, University of Minnesota, Minneapolis, Minnesota 55455, United States

Complete contact information is available at: https://pubs.acs.org/10.1021/acs.langmuir.3c01085

Notes

The authors declare no competing financial interest.

ACKNOWLEDGMENTS

The authors thank Charles Maldarelli and Ilona Krestchmar for insightful conversations. This research was supported by the U.S. National Science Foundation (Nos. 1702352 and 2032354). Portions of this work were conducted in the

Minnesota Nano Center, which is supported by the National Science Foundation through the National Nanotechnology Coordinated Infrastructure (NNCI) under Award Number ECCS-2025124.

REFERENCES

- (1) Lu, Z.; Yin, Y. Colloidal nanoparticle clusters: functional materials by design. *Chem. Soc. Rev.* **2012**, *41*, 6874–6887.
- (2) Bormashenko, E.; Fedorets, A. A.; Frenkel, M.; Dombrovsky, L. A.; Nosonovsky, M. Clustering and self-organization in small-scale natural and artificial systems. *Philos. Trans. R. Soc., A* **2020**, 378, No. 20190443.
- (3) Liu, Y.; Shen, L.; Zamansky, R.; Coletti, F. Life and death of inertial particle clusters in turbulence. *J. Fluid Mech.* **2020**, 902, No. R1.
- (4) Vignesh, K.; Tandon, S.; Kasthuri, P.; Sujith, R. I. A complex network framework for studying particle-laden flows. *Phys. Fluids* **2022**, *34*, No. 073321.
- (5) Jacobs, D. J.; Thorpe, M. F. Generic rigidity percolation: the pebble game. *Phys. Rev. Lett.* **1995**, *75*, 4051–4054.
- (6) Jacobs, D. J.; Thorpe, M. Generic rigidity percolation in two dimensions. *Phys. Rev. E* **1996**, *53*, 3682–3693.
- (7) Jacobs, D. J.; Hendrickson, B. An algorithm for two-dimensional rigidity percolation: the pebble game. *J. Comput. Phys.* **1997**, *137*, 346–365.
- (8) van Hecke, M. Jamming of soft particles: geometry, mechanics, scaling and isostaticity. *J. Phys.: Condens. Matter* **2010**, 22, No. 033101.
- (9) Papadopoulos, L.; Porter, M. A.; Daniels, K. E.; Bassett, D. S. Network analysis of particles and grains. *J. Complex Networks* **2018**, *6*, 485–565
- (10) Zhang, S.; Zhang, L.; Bouzid, M.; Rocklin, D. Z.; Del Gado, E.; Mao, X. Correlated rigidity percolation and colloidal gels. *Phys. Rev. Lett.* **2019**, *123*, No. 058001.
- (11) Henkes, S.; Quint, D. A.; Fily, Y.; Schwarz, J. M. Rigid cluster decomposition reveals criticality in frictional jamming. *Phys. Rev. Lett.* **2016**, *116*, No. 028301.
- (12) Koeze, D. J.; Tighe, B. P. Sticky matters: Jamming and rigid cluster statistics with attractive particle interactions. *Phys. Rev. Lett.* **2018**, *121*, No. 188002.
- (13) Liu, K.; Henkes, S.; Schwarz, J. Frictional rigidity percolation: A new universality class and its superuniversal connections through minimal rigidity proliferation. *Phys. Rev. X* **2019**, *9*, No. 021006.
- (14) Liu, K.; Kollmer, J. E.; Daniels, K. E.; Schwarz, J.; Henkes, S. Spongelike rigid structures in frictional granular packings. *Phys. Rev. Lett.* **2021**, *126*, No. 088002.
- (15) Behringer, R. P.; Chakraborty, B. The physics of jamming for granular materials: a review. *Rep. Prog. Phys.* **2019**, 82, No. 012601.
- (16) Cheng, X. Experimental study of the jamming transition at zero temperature. *Phys. Rev. E* **2010**, *81*, No. 031301.
- (17) Cates, M. E.; Wittmer, J. P.; Bouchaud, J.-P.; Claudin, P. Jamming, Force Chains, and Fragile Matter. *Phys. Rev. Lett.* **1998**, *81*, 1841–1844.
- (18) Bi, D.; Zhang, J.; Chakraborty, B.; Behringer, R. P. Jamming by shear. *Nature* **2011**, *480*, 355–358.
- (19) Mari, R.; Seto, R.; Morris, J. F.; Denn, M. M. Shear thickening, frictionless and frictional rheologies in non-Brownian suspensions. *J. Rheol.* **2014**, *58*, 1693–1724.
- (20) Gameiro, M.; Singh, A.; Kondic, L.; Mischaikow, K.; Morris, J. F. Interaction network analysis in shear thickening suspensions. *Phys. Rev. Fluids* **2020**, *5*, No. 034307.
- (21) Wylie, J. J.; Koch, D. L. Particle clustering due to hydrodynamic interactions. *Phys. Fluids* **2000**, *12*, 964–970.
- (22) Kolny, J.; Kornowski, A.; Weller, H. Self-organization of cadmium sulfide and gold nanoparticles by electrostatic interaction. *Nano Lett.* **2002**, *2*, 361–364.

- (23) Koos, E. Capillary suspensions: Particle networks formed through the capillary force. *Curr. Opin. Colloid Interface Sci.* **2014**, *19*, 575–584.
- (24) Cheng, X.; McCoy, J. H.; Israelachvili, J. N.; Cohen, I. Imaging the Microscopic Structure of Shear Thinning and Thickening Colloidal Suspensions. *Science* **2011**, 333, 1276–1279.
- (25) Qiao, Y.; Ma, X.; Liu, Z.; Manno, M. A.; Keim, N. C.; Cheng, X. Tuning the rheology and microstructure of particle-laden fluid interfaces with Janus particles. *J. Colloid Interface Sci.* **2022**, *618*, 241–247
- (26) Fernandez-Rodriguez, M. A.; Rodriguez-Valverde, M. A.; Cabrerizo-Vilchez, M. A.; Hidalgo-Alvarez, R. Surface activity of Janus particles adsorbed at fluid—fluid interfaces: Theoretical and experimental aspects. *Adv. Colloid Interface Sci.* **2016**, 233, 240–254.
- (27) Zhang, J.; Grzybowski, B. A.; Granick, S. Janus Particle Synthesis, Assembly, and Application. *Langmuir* **2017**, 33, 6964–6977.
- (28) Safaie, N.; Ferrier, R. C. Janus nanoparticle synthesis: Overview, recent developments, and applications. *J. Appl. Phys.* **2020**, 127, No. 170902.
- (29) Lenis, J.; Razavi, S.; Cao, K. D.; Lin, B.; Lee, K. Y. C.; Tu, R. S.; Kretzschmar, I. Mechanical Stability of Polystyrene and Janus Particle Monolayers at the Air/Water Interface. *J. Am. Chem. Soc.* **2015**, *137*, 15370–15373.
- (30) Razavi, S.; Lin, B.; Lee, K. Y. C.; Tu, R. S.; Kretzschmar, I. Impact of Surface Amphiphilicity on the Interfacial Behavior of Janus Particle Layers under Compression. *Langmuir* **2019**, *35*, 15813–15824
- (31) Correia, E. L.; Brown, N.; Razavi, S. Janus Particles at Fluid Interfaces: Stability and Interfacial Rheology. *Nanomaterials* **2021**, *11*, No. 374.
- (32) Correia, E. L.; Winter, H. H.; Razavi, S. Two-dimensional glass transition—like behavior of Janus particle—laden interface. *Rheol. Acta* **2023**, *62*, 239—251.
- (33) Hunter, T. N.; Pugh, R. J.; Franks, G. V.; Jameson, G. J. The role of particles in stabilising foams and emulsions. *Adv. Colloid Interface Sci.* **2008**, 137, 57–81.
- (34) Dickinson, E. Food emulsions and foams: Stabilization by particles. *Curr. Opin. Colloid Interface Sci.* **2010**, *15*, 40–49.
- (35) He, L.; Lin, F.; Li, X.; Sui, H.; Xu, Z. Interfacial sciences in unconventional petroleum production: from fundamentals to applications. *Chem. Soc. Rev.* **2015**, *44*, 5446–5494.
- (36) Huang, S.; Bai, L.; Trifkovic, M.; Cheng, X.; Macosko, C. W. Controlling the Morphology of Immiscible Cocontinuous Polymer Blends via Silica Nanoparticles Jammed at the Interface. *Macromolecules* **2016**, *49*, 3911–3918.
- (37) Shahin, G. T. The Stress Deformation Interfacial Rheometer. Ph.D. Thesis, University of Pennsylvania 1986.
- (38) Brooks, C. F.; Fuller, G. G.; Frank, C. W.; Robertson, C. R. An interfacial stress rheometer to study rheological transitions in monolayers at the air- water interface. *Langmuir* **1999**, *15*, 2450–2459.
- (39) Reynaert, S.; Brooks, C. F.; Moldenaers, P.; Vermant, J.; Fuller, G. G. Analysis of the magnetic rod interfacial stress rheometer. *J. Rheol.* **2008**, *52*, 261–285.
- (40) Qiao, Y.; Fan, C.; Liu, Z.; Medina, D.; Keim, N. C.; Cheng, X. Miniature magnetic rod interfacial stress rheometer for general-purpose microscopes. *J. Rheol.* **2021**, *65*, 1103–1110.
- (41) Love, J. C.; Gates, B. D.; Wolfe, D. B.; Paul, K. E.; Whitesides, G. M. Fabrication and wetting properties of metallic half-shells with submicron diameters. *Nano Lett.* **2002**, *2*, 891–894.
- (42) Park, B. J.; Brugarolas, T.; Lee, D. Janus particles at an oil—water interface. *Soft Matter* **2011**, *7*, 6413–6417.
- (43) Pieranski, P. Two-dimensional interfacial colloidal crystals. *Phys. Rev. Lett.* **1980**, *45*, 569–572.
- (44) Binks, B. P.; Murakami, R. Phase inversion of particle-stabilized materials from foams to dry water. *Nat. Mater.* **2006**, *5*, 865–869.
- (45) Guzmán, E.; Abelenda-Núñez, I.; Maestro, A.; Ortega, F.; Santamaria, A.; Rubio, R. G. Particle-laden fluid/fluid interfaces:

- physico-chemical foundations. J. Phys.: Condens. Matter 2021, 33, No. 333001.
- (46) Dietrich, K.; Volpe, G.; Sulaiman, M. N.; Renggli, D.; Buttinoni, I.; Isa, L. Active atoms and interstitials in two-dimensional colloidal crystals. *Phys. Rev. Lett.* **2018**, *120*, No. 268004.
- (47) Reynaert, S.; Moldenaers, P.; Vermant, J. Control over colloidal aggregation in monolayers of latex particles at the oil- water interface. *Langmuir* **2006**, *22*, 4936–4945.
- (48) Reynaert, S.; Moldenaers, P.; Vermant, J. Interfacial rheology of stable and weakly aggregated two-dimensional suspensions. *Phys. Chem. Chem. Phys.* **2007**, *9*, 6463–6475.
- (49) Keim, N. C.; Hass, J.; Kroger, B.; Wieker, D. Global memory from local hysteresis in an amorphous solid. *Phys. Rev. Res.* **2020**, *2*, No. 012004.
- (50) Keim, N. C.; Medina, D. Mechanical annealing and memories in a disordered solid. *Sci. Adv.* **2022**, *8*, No. eabo1614.
- (51) Liu, Z. bwtrack 2023. https://github.com/ZLoverty/bwtrack. (last accessed August 01, 2023).
- (52) Allan, D. B.; Caswell, T.; Keim, N. C.; van der Wel, C. M.; Verweij, R. W. soft-matter/trackpy; 0.6.1, 2023. (Last accessed on August 01, 2023).
- (53) Lee, D.-T.; Schachter, B. J. Two algorithms for constructing a Delaunay triangulation. Int. *J. Comput. Inf.* **1980**, *9*, 219–242.
- (54) Falk, M. L.; Langer, J. S. Dynamics of viscoplastic deformation in amorphous solids. *Phys. Rev. E* **1998**, *57*, 7192–7205.
- (55) Keim, N. C.; Arratia, P. E. Yielding and microstructure in a 2D jammed material under shear deformation. *Soft Matter* **2013**, *9*, 6222–6225.
- (56) Keim, N. C.; Arratia, P. E. Mechanical and microscopic properties of the reversible plastic regime in a 2D jammed material. *Phys. Rev. Lett.* **2014**, *112*, No. 028302.
- (57) Foss, D. R.; Brady, J. F. Structure, diffusion and rheology of Brownian suspensions by Stokesian Dynamics simulation. *J. Fluid Mech.* **2000**, *407*, 167–200.
- (58) Petkov, P. V.; Danov, K. D.; Kralchevsky, P. A. Monolayers of charged particles in a Langmuir trough: Could particle aggregation increase the surface pressure? *J. Colloid Interface Sci.* **2016**, 462, 223–234.
- (59) Keim, N. C.; Arratia, P. E. Role of disorder in finite-amplitude shear of a 2D jammed material. *Soft Matter* **2015**, *11*, 1539–1546.
- (60) Pickering, S. U. Cxcvi.—emulsions. *J. Chem. Soc. Faraday Trans.* **1907**, 91, 2001–2021.
- (61) Melle, S.; Lask, M.; Fuller, G. G. Pickering emulsions with controllable stability. *Langmuir* **2005**, 21, 2158–2162.
- (62) Wu, J.; Ma, G.-H. Recent studies of Pickering emulsions: particles make the difference. *Small* **2016**, *12*, 4633–4648.
- (63) Mewis, J.; Wagner, N. J. Thixotropy. Adv. Colloid Interface Sci. 2009, 147–148, 214–227.
- (64) Saintillan, D. Rheology of Active Fluids. *Annu. Rev. Fluid Mech.* **2018**, *50*, 563–592.
- (65) Liu, Z.; Zhang, K.; Cheng, X. Rheology of bacterial suspensions under confinement. *Rheol. Acta* **2019**, *58*, 439–451.
- (66) Szakasits, M. E.; Saud, K. T.; Mao, X.; Solomon, M. J. Rheological implications of embedded active matter in colloidal gels. *Soft Matter* **2019**, *15*, 8012–8021.
- (67) Saud, K. T.; Ganesan, M.; Solomon, M. J. Yield stress behavior of colloidal gels with embedded active particles. *J. Rheol.* **2021**, *65*, 225–239.